In general, the maximum and minimum over the interval (z_1,z_2), respectively, has to be found in order to determine Γ_i and Γ_o. Often, it is obvious from the geometry at what location z the function in Eq. (10) has its maximum or where the function in Eq. (11) has its minimum. For example, for the case depicted in Fig. 2, the minimum of the function in Eq. (11) (and, thus, $\psi_{\min}$) is obviously determined by the lower corner on the outer body where the circular cross section ends and the vertical piece begins, as indicated in the figure. If the inner body is a cylinder (or at least the obstructing part of the inner body is cylindrical), the maximization is readily carried out by looking at the projection of the vector from ds_1 to ds_2 onto a cross section of the cylinder, leading to

$$\Gamma_i = \frac{R_i^2}{r_1 r_2} - \left[\left(1-\frac{R_i^2}{r_1^2}\right)\left(1-\frac{R_i^2}{r_2^2}\right)\right]^{\frac{1}{2}} \tag{12}$$

Even for somewhat more complicated geometries such as the one in Fig. 2, this relationship may be employed: no vector from dA_1 to dA_2 with a positive $\cos\beta_2$ (i.e., hitting dA_2 from the top) could intersect either one of the conical pieces, but it could intersect the cylinder, making Eq. (12) valid. This is indicated in Fig. 2 as $\psi = \cos^{-1}\Gamma_i$; in the present case, this angle is larger than the $\psi_{\max}$ determined from the $\cos\beta_2 > 0$ condition, and therefore, does not apply.

In summary, the radiation shape factor between two strips located on the same or opposite surfaces of two concentric axisymmetric bodies is determined by Eqs. (7) and (8) with the limiting values $\cos\psi_{\max}$ and $\cos\psi_{\min}$ taking on the values ϕ_1, ϕ_2, Γ_i, and Γ_o depending on the location and orientation of the strips. A detailed listing of the values for $\cos\psi_{\max}$ and $\cos\psi_{\min}$ for all situations is given in Table 1. Only those combinations of values for ϕ_1 and ϕ_2 are included in the table that result in nonzero shape factors (for example, if $\cos\theta_1 > 0$ and $\cos\theta_2 > 0$, the strips cannot see each other at all if $\phi_1 > 1$ and $\phi_2 > 1$).

As an additional numerical example, consider the case of an infinitesimal strip on a cylinder and a second strip on a disk attached perpendicularly to the cylinder (Fig. 3). This corresponds to the special case of circular-finned cylinders for which Masuda[7] has already given analytical expressions. For a cylinder as the inner axisymmetric body, we have $\theta_1 = 0$ and, for a horizontal fin (above ds_1, pointing down), we have $\theta_2 = \pi/2$. With $\Delta z = z_2 - z_1 > 0$, we have $\phi_1 = r_1/r_2$ and $\phi_2 \to \pm\infty$ (for $\theta_2 = \pi/2 \pm 0$). There are no obstructions between the two strips, so Γ_i and Γ_o do not apply. It follows from Table 1 that $\cos\psi_{\min} = 1$ and $\cos\psi_{\max} = \phi_1$ (note that both $\cos\theta_2 \geq 0$ with $\phi_2 \to -\infty$ and $\cos\theta_2 \leq 0$ with $\phi_2 \to +\infty$ lead to the same result). For $\psi_{\min} = 0$ it follows that $B(\alpha,\phi_1,\phi_2,\cos\psi_{\min}=1) = 0$ and

$$\lim_{\theta_2 \to 0} \cos\theta_2 B(\alpha,\phi_1,\phi_2,\cos\psi_{\max}=\phi_1) = \frac{\Delta z}{r_1}\left\{\frac{(1-\phi_1^2)^{\frac{1}{2}}}{\alpha^2-1} + 2\frac{1-\alpha\phi_1}{(\alpha^2-1)^{3/2}}\tan^{-1}\left[\left(\frac{\alpha+1}{\alpha-1}\frac{1-\phi_1}{1+\phi_1}\right)^{\frac{1}{2}}\right]\right\}$$

Thus, the shape factor is

$$dF_{d1-d2} = \frac{\Delta z\, ds_2}{2\pi r_1^2}\left\{\frac{(1-\phi_1^2)^{\frac{1}{2}}}{\alpha^2-1} + 2\frac{1-\alpha\phi_1}{(\alpha^2-1)^{3/2}}\tan^{-1}\left[\left(\frac{\alpha+1}{\alpha-1}\frac{1-\phi_1}{1+\phi_1}\right)^{\frac{1}{2}}\right]\right\} \tag{13}$$

It is readily verified that this formula is identical to Eq. (13) in the paper by Masuda.

Conclusion

A simple analytical formula has been given for the radiative shape factor between any two ring strips placed on two arbitrarily shaped concentric axisymmetric bodies. This approach eliminates the need for one numerical quadrature with obstruction checking for radiative heat-transfer calculations in such geometries.

Acknowledgment

This work was carried out while the author was on leave at the Institut für Reaktorbauelemente, Kernforschungszentrum Karlsruhe, Federal Republic of Germany.

References

[1]Siegel, R. and Howell, J. R., *Thermal Radiation Heat Transfer*, 2nd ed., McGraw-Hill, New York, 1980.

[2]Howell, J. R., *A Catalog of Radiation Configuration Factors*, McGraw-Hill, New York, 1982.

[3]Morizumi, S. J., "Analytical Determination of Shape Factors from a Surface Element to an Axisymmetric Surface," *AIAA Journal*, Vol. 2, Nov. 1964, pp. 2028–2030.

[4]Robbins, W. H. and Todd, C. A., "Analysis, Feasibility and Wall-Temperature Distribution of a Radiation-Cooled Nuclear-Rocket Nozzle," NASA TN D-818, 1962.

[5]Chung, B. T. F. and Naraghi, M. H. N., "A Simpler Formulation for Radiative View Factors from Spheres to a Class of Axisymmetric Bodies," *Transactions of ASME, Journal of Heat Transfer*, Vol. 104, 1982, pp. 201–204.

[6]Chung, B. T. F. and Naraghi, M. H. N., "Some Exact Solutions for Radiative View Factors from Spheres," *AIAA Journal*, Vol. 19, Aug. 1981, pp. 1077–1081.

[7]Masuda, H., "Radiant Heat Transfer on Circular-Finned Cylinders," *Reports of the Institute of High Speed Mechanics, Tohoku University*, Japan, Vol. 27, 1973, pp. 67–89.

Perturbation Solution for Spherical Solidification by Convective Cooling

Luiz F. Milanez*
and José L. Boldrini†
Universidade Estadual de Campinas
São Paulo, Brazil

Nomenclature

c	= specific heat of solid material
h	= heat transfer coefficient
k	= thermal conductivity of solid material
L	= latent heat of fusion
R	= radial position in the solidified material
R_f	= radial position of the freezing front
R_0	= radius of sphere
T	= temperature in the solidified material
T_f	= freezing temperature
T_∞	= temperature of cooling fluid
t	= time
α	= thermal diffusitivity of solid material
ρ	= density of solid material

Introduction

THE problem of the inward solidification of spheres has received considerable attention in the literature.[1-5] The

Received Oct. 21, 1986; revision received Feb. 12, 1987; presented as Paper 87-1493 at the AIAA 22nd Thermophysics Conference, June 8-10, 1987.

*Associate Professor, Department of Mechanical Engineering.
†Assistant Professor, Department of Applied Mathematics.

method of perturbation expansion is still a useful approximate analytical tool for heat transfer analysis, despite the explosive growth of numerical computation involving finite differences. The use of the regular perturbation method to obtain the solution of this problem leads to an expression for the freezing time that is singular at the origin.[3] In order to obtain a uniformly valid solution, the method of strained coordinates is used in a similar way as was employed by Pedroso and Domoto[4] for inward spherical solidification with the wall temperature assumed constant. However, in the case of convective cooling, the equations are more involved. A solution with correction up to the first order in an asymptotic expansion using the Stefan number as a parameter is presented and compared with numerical results.

Analysis

Consider a sphere of radius R_0 initially containing liquid at its freezing temperature T_f being suddenly cooled by a fluid at constant temperature T_∞ with a heat transfer coefficient h. This configuration is illustrated in Fig. 1. The properties of the solidified material are assumed as constants. The heat flow within the frozen spherical shell is governed by the transient heat conduction equation

$$\frac{\partial T}{\partial t}=\frac{\alpha}{R}\frac{\partial^2(RT)}{\partial R^2} \qquad R_f\le R\le R_0 \tag{1}$$

subjected to the boundary conditions

$$T(R,t)=T_f \qquad 0\le R\le R_f \tag{2}$$

$$-k\frac{dT}{dR}=h(T-T_\infty) \qquad R=R_0 \tag{3}$$

An energy balance at the freezing front yields

$$\frac{dR}{dt}=\frac{k}{\rho L}\frac{\partial T}{\partial R} \qquad R=R_f \tag{4}$$

It is convenient to introduce the dimensionless variables

$$\theta=\frac{T-T_\infty}{T_f-T_\infty} \quad \tau=\frac{k(T_f-T_\infty)t}{\rho L R_0^2} \quad r=\frac{R}{R_0} \quad r_f=\frac{R_f}{R_0} \tag{5}$$

and the dimensionless physical parameters

$$\epsilon=\frac{c(T_f-T_\infty)}{L} \qquad \text{Stefan number} \tag{6}$$

$$Bi=\frac{hR_0}{k} \qquad \text{Biot number}$$

Rewriting Eqs. (1-4) in terms of the new parameters, after changing variables from (τ,r) to (r_f,r), the normalized form of the boundary-value problem becomes

$$\epsilon\frac{\partial\theta}{\partial r_f}\left.\frac{\partial\theta}{\partial r}\right|_{r=r_f}=\frac{1}{r}\frac{\partial^2(r\theta)}{\partial r^2} \tag{7}$$

$$\theta(r_f, r=r_f)=1 \tag{8}$$

$$\theta(r_f,r=1)=-\frac{1}{Bi}\left.\frac{\partial\theta}{\partial r}\right|_{r=1} \tag{9}$$

$$\frac{dr_f}{d\tau}=-\left.\frac{\partial\theta}{\partial r}\right|_{r=r_f} \tag{10}$$

In order to solve the preceding set of equations, the strained coordinates method is considered and two new independent variables, ϕ and ψ, are introduced, as in Ref. 4:

$$r=r(\psi,\phi;\epsilon)=\phi+\sum_{j=1}^{\infty}\epsilon^j\sigma_j(\psi,\phi) \tag{11}$$

$$r_f=r_f(\psi,\epsilon)=\psi+\sum_{j=1}^{\infty}\epsilon^j\sigma_j(\psi,\phi=\psi) \tag{12}$$

For all j it is required that σ_j be smooth and

$$\lim_{\phi\to 1}\sigma_j(\psi,\phi)=0 \tag{13}$$

That is, that the preceding transformations be perturbations of the identity at $\phi=1$. To comply with the boundary conditions, other requirements will be introduced by the perturbation argument used to find the normalized temperature as well as the functions σ_j.

After changing variables from (r_f,r) to (ψ,ϕ) in Eqs. (7-10), the normalized temperature distribution taken as a function of the variables ϕ,ψ and of the parameter ϵ can be expanded as

$$\theta(\psi,\phi;\epsilon)=\sum_{j=0}^{\infty}\epsilon^j\theta_j(\psi,\phi) \tag{14}$$

After collecting terms of the same powers of ϵ, the zeroth-order boundary-value problem is found to be

$$\frac{\partial^2(\phi\theta_0)}{\partial\phi^2}=0 \tag{15}$$

$$\theta_0(\psi,\phi=\psi)=1 \tag{16}$$

$$\theta_0(\psi,\phi=1)=-\frac{1}{Bi}\left.\frac{\partial\theta_0}{\partial\phi}\right|_{\phi=1} \tag{17}$$

which can be solved to obtain

$$\theta_0(\psi,\phi)=\frac{1}{\psi(1-Bi)+Bi}\left[(1-Bi)\psi+\frac{Bi\psi}{\phi}\right] \tag{18}$$

The first-order boundary-value problem can then be written as

$$\frac{1}{\phi}\frac{\partial^2}{\partial\phi^2}(\phi\theta_1)-\frac{2\sigma_1}{\phi^2}\frac{\partial\theta_0}{\partial\phi}-\frac{2}{\phi}\frac{\partial\theta_0}{\partial\phi}\frac{\partial\sigma_1}{\partial\phi}-2\frac{\partial\sigma_1}{\partial\phi}\frac{\partial^2\theta_0}{\partial\phi^2}$$

$$-\frac{\partial\theta_0}{\partial\phi}\frac{\partial^2\sigma_1}{\partial\phi^2}=\frac{\partial\theta_0}{\partial\psi}\left(\left.\frac{\partial\theta_0}{\partial\phi}\right|_{\phi=\psi}\right) \tag{19}$$

$$\theta_1(\psi,\phi=\psi)=0 \tag{20}$$

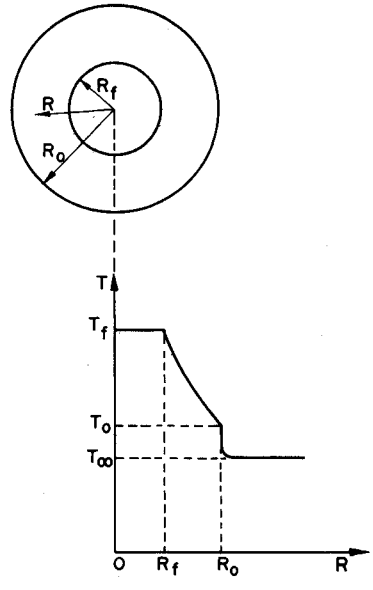

Fig. 1 Sphere cross section.

$$\theta_1(\psi,\phi=1)=-\frac{1}{Bi}\left(\frac{\partial\theta_1}{\partial\phi}-\frac{\partial\sigma_1}{\partial\phi}\frac{\partial\theta_0}{\partial\phi}\right)\Bigg|_{\phi=1} \tag{21}$$

Now σ_1 will be chosen such that $\theta_1\equiv 0$, and the second boundary condition requires

$$\frac{\partial\sigma_1}{\partial\phi}\Bigg|_{\phi=1}=0.$$

The consideration of Eqs. (18–21) results in

$$\phi^2\frac{\partial^2\sigma_1}{\partial\phi^2}-2\phi\frac{\partial\sigma_1}{\partial\phi}+2\sigma_1=-\frac{Bi[(1-Bi)\phi^4+Bi\phi^3]}{\psi^2[\psi(1-Bi)+Bi]^2} \tag{22}$$

$$\sigma_1(\psi,\phi=1)=0 \tag{23}$$

$$\frac{\partial\sigma_1}{\partial\phi}(\psi,\phi=1)=0 \tag{24}$$

Since Eq. (22) is a forced Euler equation, the problem can be solved to give

$$\sigma_1(\psi,\phi)=\frac{Bi}{\psi^2[\psi(1-Bi)+Bi]^2}\left[-\frac{(2+Bi)}{6}\phi+\frac{(1+Bi)}{2}\phi^2-\frac{Bi}{2}\phi^3-\frac{(1-Bi)}{6}\phi^4\right] \tag{25}$$

The preceding procedure of successively determining σ_j by requiring that $\theta_j\equiv 0$ in principle can be applied to any order, always resulting in forced Euler equations (with the same left side as shown). However the solutions will be restricted up to the first order only.

In order to find the freezing time, Eq. (10) is rewritten in terms of ψ and ϕ to obtain

$$\frac{d\tau}{d\psi}=\frac{dr_f}{d\psi}\left(\frac{\partial\theta}{\partial\phi}\frac{\partial\phi}{\partial r}\right)^{-1}\Bigg|_{\phi=\psi} \tag{26}$$

By using the previous results, after an integration with respect to ψ and the use of the condition $\tau=0$ when $\psi=1$, we obtain

$$\tau=b_0(Bi,\psi)+\epsilon b_1(Bi,\psi)+O(\epsilon^2) \tag{27}$$

where

$$b_0(1,\psi)=\tfrac{1}{2}(1-\psi^2) \tag{28}$$

$$b_1(1,\psi)=1-2\psi+\psi^2 \tag{29}$$

and, when $Bi\neq 1$,

$$b_0(Bi,\psi)=\frac{1}{2}(1-\psi^2)+\frac{(1-Bi)}{3Bi}(1-\psi^3) \tag{30}$$

$$b_1(Bi,\psi)=\frac{Bi^2-3}{3(1-Bi)^2}+\frac{2Bi}{3(1-Bi)}\psi+\frac{\psi^2}{3}+\frac{2}{3(1-Bi)^2}\frac{1}{[\psi(1-Bi)+Bi]} \tag{31}$$

From this, the solidification front velocity can be derived as

$$\frac{dr_f}{d\tau}=\left(\frac{dr_f}{d\psi}\right)\left(\frac{d\tau}{d\psi}\right)^{-1} \tag{32}$$

Results and Discussion

A first-order perturbation solution has been obtained for the inward solidification of a saturated liquid inside a spherical container using the Stefan number ϵ, the ratio of the sensible heat to the latent heat, as the perturbation parameter. Results from the given solution are presented graphically and compared with numerical results[2] in Figs. 2–5.

The normalized freezing front position as function of time is calculated as follows. For each pair of Stefan and Biot numbers, by assuming values successively smaller than unity for ψ, in Eq. (12) up to order ϵ, together with the expression for σ_1 in Eq. (25), the freezing front location r_f can be determined. The corresponding normalized time can be obtained from Eq. (27) until the value of r_f tends to zero. Figures 2 and 3 show the solidification front motion with time for $\epsilon=0.5$ and $\epsilon=2.0$ for different values of the Biot number. As expected, the analytical results are in good agreement with the numerical solutions for $\epsilon<1$. The accuracy of the solution increases as ϵ, the perturbation parameter, becomes smaller.

The temperature distribution in the solidified material is obtained by using Eq. (18) together with Eqs. (11) and (12) with the expression for σ_1 given by Eq. (25). For given Stefan and Biot numbers, Eq. (12) relates ψ to the freezing front location r_f. To know the temperature distribution in this solidified material of thickness $1-r_f$, values between 1 and ψ are assigned to ϕ in Eqs. (11) and (18) obtaining r and θ respectively. Figures 4 and 5 show the temperature profile in the solid phase for different positions of the interface. Again it can be seen that the agreement with numerical solutions is very good and that the smaller the Stefan number, the greater the accuracy of the results.

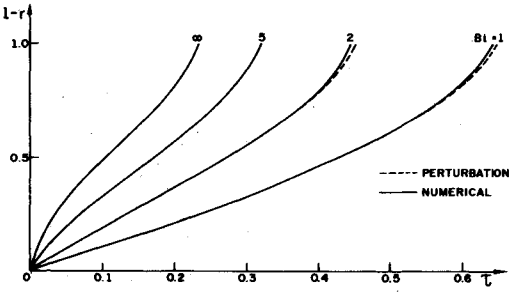

Fig. 2 Solidification front motion with time for $\epsilon=0.5$.

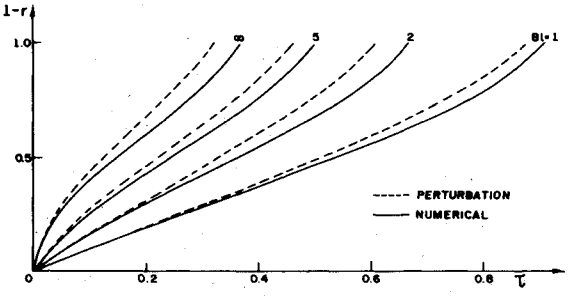

Fig. 3 Solidification front motion with time for $\epsilon=2.0$.

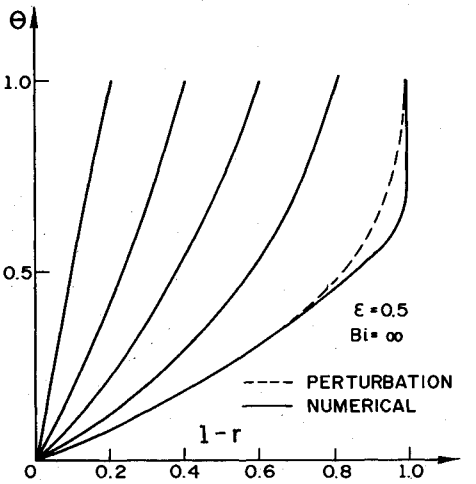

Fig. 4 Solid phase temperature profile for different interface positions.

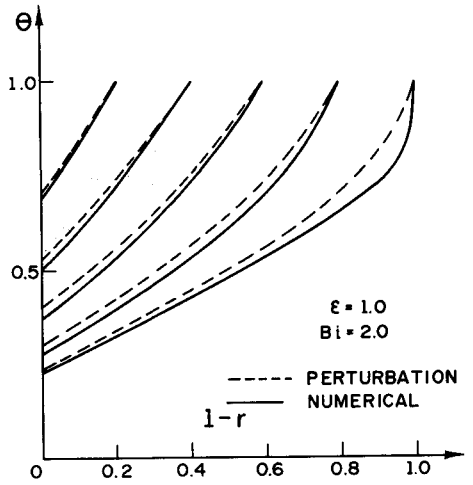

Fig. 5 Solid phase temperature profile for different interface positions.

References

[1]Tao, L.C., "Generalized Numerical Solutions of Freezing a Saturated Liquid in Cylinders and Sphere," *AIChE Journal,* Vol. 13, Jan. 1967, pp. 165-169.

[2]Milanez, L.F. and Ismail, K.A.R., "Inward Solidification of Spheres: Numerical and Experimental Analysis," ASME Paper 84-WA/HT-9, 1984.

[3]Huang, C.L. and Shih, Y.P., "A Perturbation Method for Spherical and Cylindrical Solidification," *Chemical Engineering Science,* Vol. 30, 1975, pp. 897-906.

[4]Pedroso, R.I. and Domoto, G.A., "Inward Spherical Solidification-Solution by the Method of Strained Coordinates," *International Journal of Heat Mass Transfer,* Vol. 16, 1973, pp. 1037-1043.

[5]Kucera, A. and Hill, J.M., "On Inward Solidifying Cylinders and Spheres Initially Not at Their Fusion Temperature," *International Journal of Non-Linear Mechanics,* Vol. 21, No. 1, 1986, pp. 73-82.

Roll-Out-Fin Expandable Space Radiator Concept

R. Ponnappan*
Universal Energy Systems, Dayton, Ohio
and
J. E. Beam† and E. T. Mahefkey‡
Aero Propulsion Laboratory
Wright-Patterson Air Force Base, Ohio

Nomenclature

a = area of cross section
A = external area exposed to space
b = width of the roll-out fin
C_p = specific heat capacity at constant pressure
$\dot{E}$ = rate of energy storage
F = spring force
h = fin wall thickness
h_f = specific enthalpy of fluid
h_{fg} = specific enthalpy of vaporization of the fluid
m = radiator mass
$\dot{m}$ = mass flow rate
P = pressure inside the fin
$\dot{Q}$ = heat rate
t = time
T = temperature
ΔT = temperature difference
u_g = specific internal energy
V = volume
$\dot{W}$ = rate of work done
x = length of deployment of the fin
α, β = parameters defined in Eqs. (3) and (4)
ϵ = emissivity
ρ = density
σ = Stefan-Boltzmann constant
τ = time constant

Subscripts

c = condensate
f = fin
i = input
s = sink
v = vapor

Received May 15, 1986; Presented as Paper 86-1323 at the AIAA/ASME 4th Thermophysics and Heat Transfer Conference, Boston, MA, June 2-4, 1986; revision received Sept. 23, 1986.

*Senior Scientist, Scientific Services Division. Member AIAA.

†Project Engineer, Nuclear/Thermal Technical Area. Member AIAA.

‡Technical Area Manager, Power Technology Branch. Member AIAA.

Introduction

WASTE heat rejection in space at temperatures of 300-423 K is posing technological problems for spacecraft of 100 kW capacity or more. Difficult thermal management problems lie with the high-power, low-temperature waste heat rejection associated with power processing and the payload electronic component cooling.[1] This necessitates the development of lightweight deployable radiators for future spacecraft. There are several different space radiator concepts discussed in the literature.[2-7] These concepts range from the conventional fluid loop system to the more advanced liquid droplet radiators (LDR), depending upon the temperature range and power dissipation requirements. The mass-to-power ratios $m/\dot{Q}$ of the radiators (defined as the ratio of the radiator mass to its radiating power level) are 0.017-20 kg/kW for various systems. Most of the relatively newer ideas (such as rotating spherical balloon, dust particle, glass filament, liquid droplet, direct contact belt, and single-phase external liquid flow radiators) are still in the conceptual stage. The low- or room-temperature systems have very high (orders of magnitude) mass-to-power ratios compared to the liquid metal temperature range systems.

The expandable radiator of the roll-out fin type shown in Fig. 1 contains internal vapor space and liquid condensate return channels that are primed via capillary action and the roll-up action of the spring-loaded, thin-walled, vapor chamber segments.[8] The heat transport is accomplished through the evaporation and condensation processes, while the deployment and the roll-up operations relied on the working fluid (vapor) pressure and the spring stiffness, respectively. The life expectancy of the radiator in low Earth orbits is affected by the micrometeoroid impacts. Separate research studies on survivability are required. Armor cover for the radiator in stored position, self-sealing fluid or fluid loss minimization in case of puncture, and closed-type modular fins are some of the problems to be solved. In the present study, only the feasibility of the roll-out fin concept is investigated.

Roll-Out Fin Radiator Concept

The roll-out fin radiator system can be conceived as a panel made of a number of fins mechanically working in parallel. The individual tubular segments are capable of working independently in a given pulsed (intermittant) or steady heat input condition. A group of such panels can be arranged around a vapor header as seen in Fig. 1 to form a radiator system. Two arrangements are possible to couple the fins to the primary thermal load via the vapor header. One method is the direct contact coupling where the primary fluid in the vapor header